

Hydrodynamic Coupling of Two Brownian Spheres to a Planar Surface

Eric R. Dufresne⁽¹⁾, Todd M. Squires⁽²⁾, Michael P. Brenner⁽³⁾, and David G. Grier⁽¹⁾

⁽¹⁾*Dept. of Physics, James Franck Institute, and Institute for Biophysical Dynamics
The University of Chicago, Chicago, IL 60637*

⁽²⁾*Dept. of Physics, Harvard University, Cambridge, MA 02138*

⁽³⁾*Dept. of Mathematics, Massachusetts Institute of Technology, Cambridge, MA 02139*
(October 30, 2018)

We describe direct imaging measurements of the collective and relative diffusion of two colloidal spheres near a flat plate. The bounding surface modifies the spheres' dynamics, even at separations of tens of radii. This behavior is captured by a stokeslet analysis of fluid flow driven by the spheres' and wall's no-slip boundary conditions. In particular, this analysis reveals surprising asymmetry in the normal modes for pair diffusion near a flat surface.

Despite considerable progress over the past two centuries [1] hydrodynamic properties of all but the simplest colloidal systems remain controversial or unexplained. For example, velocity fluctuations in sedimenting colloidal suspensions are predicted to diverge with system size [2]. Experimental observations indicate, on the other hand, that long-wavelength fluctuations are suppressed by an as-yet undiscovered mechanism [3–5]. One possible explanation is that hydrodynamic coupling to bounding surfaces may influence particles' motions to a greater extent and over a longer range than previously suspected [6]. Such considerations invite a renewed examination of how hydrodynamic coupling to bounding surfaces influences colloidal particles' dynamics.

This Letter describes an experimental and theoretical investigation of two colloidal spheres' diffusion near a flat plate. Related studies have addressed the dynamics of two spheres far from bounding walls [7,8], and of a single sphere in the presence of one or two walls [9]. Confinement by two walls poses particular difficulties since available theoretical predictions apply only for highly symmetric arrangements [10], or else contradict each other [11,12]. The geometry we have chosen avoids some of this complexity while still highlighting the range of non-additive hydrodynamic coupling in a many-surface system.

We combined optical tweezer manipulation [13] and digital video microscopy [14] to measure four components of the pair diffusion tensor for two colloidal spheres as a function of their center-to-center separation r and of their height h above a planar glass surface. Measurements were performed on silica sphere of radius $0.495 \pm 0.025 \mu\text{m}$ (Duke Scientific lot 21024) dispersed in a layer of water $140 \pm 2 \mu\text{m}$ thick. The suspension was sandwiched between a microscope slide and a #1 coverslip whose surfaces were stringently cleaned before assembly [15] and whose edges were hermetically sealed with a uv cured epoxy (Norland type 88) to prevent evaporation and suppress bulk fluid flow. A transparent thin film heater

bonded to the microscope slide and driven by a Lakeshore LM-330 temperature controller maintained the sample volume's temperature at $T = 29.00 \pm 0.01^\circ\text{C}$, as measured by a platinum resistance thermometer. The addition of 2 mM of NaCl to the solution minimized electrostatic interactions among the weakly charged spheres and glass surfaces by reducing the Debye screening length to 2 nm. Under these conditions, the individual spheres' free self-diffusion coefficients are expected to be $D_0 = k_B T / (6\pi\eta a) = 0.550 \pm 0.028 \mu\text{m}^2/\text{sec}$, where $\eta = 0.817 \text{ cP}$ is the electrolyte's viscosity [16].

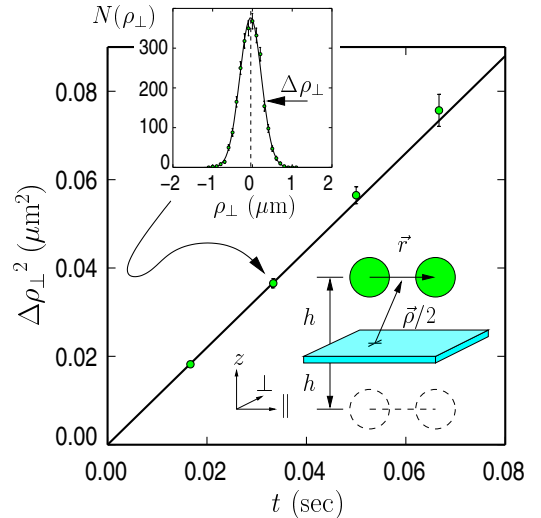


FIG. 1. Measurement of a typical pair diffusion coefficient in the geometry depicted in the lower inset. Dashed spheres represent hydrodynamic images. The upper inset shows the histogram of two spheres' collective displacements in the \perp direction starting from $h = 25.5 \pm 0.7 \mu\text{m}$, $r = 7.00 \pm 0.25 \mu\text{m}$, and $\rho = 0$, after free diffusion for $\tau = 1/30 \text{ sec}$. Fitting to a Gaussian yields the rms displacement $\Delta\rho_{\perp}(r, h, \tau)$. The main plot tracks the evolution of $\Delta\rho_{\perp}^2(r, h, \tau)$ together with a least squares fit to Eq. (1) for the diffusion coefficient $D_{\perp}^C(r, h)$. The result is indicated by an arrow in Fig. 2(d).

The spheres' motions were tracked with an Olympus

IMT-2 optical microscope using a $100\times$ NA 1.4 oil immersion objective. Images acquired with an NEC TI-324A CCD camera were recorded on a JVC-822DXU SVHS video deck before being digitized with a Mutech MV-1350 frame grabber at 1/60 sec intervals. Field-accurate digitization was assured by interpreting the vertical interlace time code recorded onto each video field. The spheres' locations $\vec{r}_1(t)$ and $\vec{r}_2(t)$ in the image acquired at time t then were measured to within 20 nm using a computerized centroid tracking algorithm [14].

A pair of spheres was placed reproducibly in a plane parallel to the glass surfaces using optical tweezers [13]. These optical traps were created with a solid state laser (Coherent Verdi) whose beam was brought to a focus within the sample volume by the microscope's objective. Resulting optical gradient forces suffice to localize a silica sphere at the focal point despite random thermal forces [13]. Two optical traps were created by alternating the focused laser spot between two positions in the focal plane at 200 Hz using a galvanometer-driven mirror [17]. Diverting the trapping laser onto a beam block every few cycles freed the spheres to diffuse away from this well defined initial condition. Resuming the trap's oscillation between the two trapping points resets the spheres' positions. Alternately trapping and releasing the spheres allowed us to sample their dynamics efficiently in a particular geometry. Allowing the spheres only $\tau = 83$ msec (5 video fields) of freedom before retrapping them for 16 msec (less than 1 video field) ensured that their out-of-plane motions, $\Delta z < \sqrt{2D_0\tau} = 0.4 \mu\text{m}$, cause negligible tracking errors.

Because optical tweezers form in the microscope's focal plane, their height h relative to the coverslip's surface can be adjusted from 1 to $30 \mu\text{m}$ with $0.5 \mu\text{m}$ accuracy by adjusting the microscope's focus. For a given height, we continuously varied the spheres' initial separation between $2 \mu\text{m}$ and $10 \mu\text{m}$ at 0.025 Hz for a total of 20 minutes. This procedure yielded 60,000 samples of the spheres' dynamics in 1/60 sec intervals divided into sequences 5/60 sec long for each value of h . These trajectory data were decomposed into cooperative motions $\vec{\rho} = \vec{r}_1 + \vec{r}_2$ and relative motions $\vec{r} = \vec{r}_1 - \vec{r}_2$ either perpendicular or parallel to the initial separation vector, and binned according to the initial separation, r . The diffusion coefficients $D_\psi(r, h)$ associated with each mode of motion $\psi(r, h, \tau)$ at each height and initial separation were then obtained from the Stokes-Einstein formula

$$\langle \Delta\psi^2(\tau) \rangle = 2D_\psi(r, h)\tau, \quad (1)$$

where the angle brackets indicate an ensemble average.

Fig. 1 shows typical data for one mode of motion at one height and starting separation. Diffusion coefficients $D_\psi(r, h)$ extracted from least squares fits to Eq. (1) appear in Fig. 2 as functions of r for the smallest and largest accessible values of h . The horizontal dashed lines in

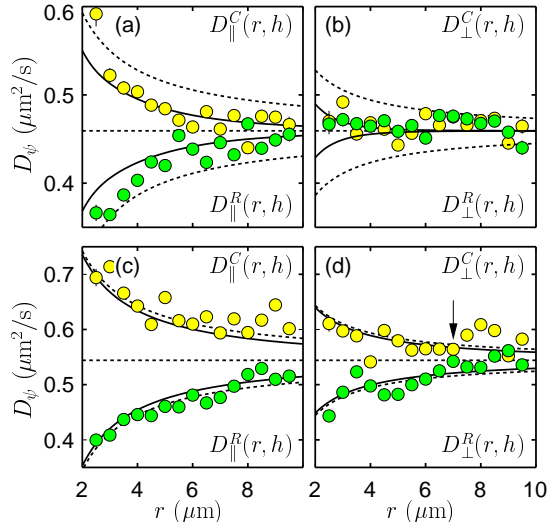


FIG. 2. Pair diffusion coefficients for $1 \mu\text{m}$ diameter silica spheres as a function of center-to-center separation r and at two different center-to-surface heights h . (a) and (b): $h = 1.55 \pm 0.66 \mu\text{m}$. (c) and (d): $h = 25.5 \pm 0.7 \mu\text{m}$. (a) and (c): Collective and relative motions parallel to the initial separation vector. (b) and (d): Perpendicular. Dashed curves result from linear superposition of drag coefficients. Solid curves result from the theory described here, with no adjustable parameters. Horizontal dashed lines indicate the asymptotic self-diffusion coefficient $D_{xy}(h)$ from Eq. (11).

Fig. 2 indicate the spheres' asymptotic self-diffusion coefficients. Measurements' deviations from these limiting values reveal the influence of the spheres' hydrodynamic interactions.

Particles moving through a fluid at low Reynolds number excite large-scale flows through the no-slip boundary condition at their surfaces. These flows couple distant particles' motions, so that each particle's dynamics depends on the particular configuration of the entire collection. This dependence is readily calculated using Batchelor's generalization of Einstein's classic argument [18]: The probability to find N particles at equilibrium in a particular configuration $\{\vec{r}_1, \dots, \vec{r}_N\}$ depends on their interaction $\Phi(\vec{r}_1, \dots, \vec{r}_N)$ through Boltzmann's distribution, $P(\vec{r}_1, \dots, \vec{r}_N) = \exp[-\Phi/(k_B T)]$. The corresponding force $-\nabla\Phi = k_B T \nabla P/P$ drives a probability flux $k_B T \mathbf{b} \nabla P$, where $\mathbf{b}(\vec{r}_1, \dots, \vec{r}_N)$ is the particles' mobility tensor. The system reaches equilibrium when this interaction-driven flux is balanced by a diffusive flux $-\mathbf{D} \nabla P$. It follows that the N -particle diffusivity is $\mathbf{D} = k_B T \mathbf{b}$. Elements of \mathbf{D} lead to generalized Stokes-Einstein relations [19]

$$\langle \Delta r_{i\alpha}(\tau) \Delta r_{j\beta}(\tau) \rangle = 2D_{i\alpha, j\beta} \tau. \quad (2)$$

describing how particle i 's motion in the α direction couples to particle j 's in the β direction.

The mobility tensor for spheres of radius a has the form

$$b_{i\alpha,j\beta} = \frac{\delta_{i\alpha,j\beta}}{6\pi\eta a} + b_{i\alpha,j\beta}^e \quad (3)$$

$b_{i\alpha,j\beta}^e$ is the Green's function for the flow at \vec{r}_i in the α direction due to an external force at \vec{r}_j in the β direction. In the present discussion, it accounts for no-slip boundary conditions at all other surfaces in the system.

If the spheres are well separated, we may approximate the flow field around a given sphere by a stokeslet, the flow due a point force at the sphere's location. This approximation is valid to leading order in the spheres' radius. The Green's function for the flow at \vec{x} in the α direction due to a stokeslet at \vec{r}_j in the β direction is [20]

$$G_{\alpha\beta}^S(\vec{x} - \vec{r}_j) = \frac{1}{8\pi\eta} \left[\frac{\delta_{\alpha\beta}}{|\vec{x} - \vec{r}_j|} + \frac{(\vec{x} - \vec{r}_j)_\alpha (\vec{x} - \vec{r}_j)_\beta}{|\vec{x} - \vec{r}_j|^3} \right] \quad (4)$$

so that $b_{i\alpha,j\beta}^e = G_{\alpha\beta}^S(\vec{r}_i - \vec{r}_j)$. In the particular case of two identical spheres, diagonalizing the resulting diffusivity tensor \mathbf{D} yields the diffusion coefficients for two collective (C) modes and two relative (R) modes along directions perpendicular (\perp) and parallel (\parallel) to the initial separation [18]

$$\frac{D_{\perp}^{C,R}(r)}{D_0} = 1 \pm \frac{3}{4} \frac{a}{r} + \mathcal{O}\left(\frac{a^3}{r^3}\right) \quad (5)$$

$$\frac{D_{\parallel}^{C,R}(r)}{D_0} = 1 \pm \frac{3}{2} \frac{a}{r} + \mathcal{O}\left(\frac{a^3}{r^3}\right), \quad (6)$$

where the positive corrections apply to collective modes and the negative to relative. The collective diffusion coefficients D_{\perp}^C and D_{\parallel}^C are enhanced by hydrodynamic coupling because fluid displaced by one sphere entrains the other. Relative diffusion coefficients D_{\perp}^R and D_{\parallel}^R are suppressed, on the other hand, by the need to transport fluid into and out of the space between the spheres.

Introducing a planar boundary into this system adds considerable complexity. The flow field around a small sphere located a height h above a horizontal wall is most easily calculated by the method of images [21], in which the wall's no-slip boundary condition is satisfied by placing a stokeslet (S), a source doublet (D), and a stokeslet doublet (SD) a distance h below the plane of the wall [21,20]. The flow due to this image system is described by the Green's function

$$G_{\alpha\beta}^W(\vec{x} - \vec{R}_j) = -G_{\alpha\beta}^S(\vec{x} - \vec{R}_j) + 2h^2 G_{\alpha\beta}^D(\vec{x} - \vec{R}_j) - 2h G_{\alpha\beta}^{SD}(\vec{x} - \vec{R}_j) \quad (7)$$

where $\vec{R}_j = \vec{r}_j - 2h\hat{z}$ is the position of sphere j 's image, and

$$G_{\alpha\beta}^D(\vec{y}) = (1 - 2\delta_{\alpha z}) \frac{\partial}{\partial y_\beta} \left(\frac{y_\alpha}{y^3} \right) \quad (8)$$

$$G_{\alpha\beta}^{SD}(\vec{y}) = (1 - 2\delta_{\alpha z}) \frac{\partial}{\partial y_\beta} G_{\alpha z}^S(\vec{y}) \quad (9)$$

are Green's functions for a source dipole and a stokeslet doublet, respectively. The flow field set up by the image system (and thus by the wall's no-slip boundary condition) entrains the sphere through $b_{i\alpha,i\beta}^e = G_{\alpha\beta}^W(\vec{r}_i - \vec{R}_i)$ and decreases its mobility. Two independent modes emerge from this analysis, one (z) normal to the wall and the other (xy) parallel, with diffusivities [10]

$$\frac{D_z(h)}{D_0} = 1 - \frac{9}{8} \frac{a}{h} + \mathcal{O}\left(\frac{a^3}{h^3}\right) \quad (10)$$

$$\frac{D_{xy}(h)}{D_0} = 1 - \frac{9}{16} \frac{a}{h} + \mathcal{O}\left(\frac{a^3}{h^3}\right). \quad (11)$$

Eqs. (5) and (6) should suffice for two spheres far from bounding surfaces. Similarly, the spheres' motions should decouple when the influence of a nearby wall dominates; Eqs. (10) and (11) then should apply. At intermediate separations, however, neither set of formulas is accurate. Naively adding the drag coefficients due to sphere-sphere and sphere-wall interactions yields $D_{\psi}^{-1}(r, h) = D_{\psi}^{-1}(r) + D_{xy}^{-1}(h) - D_0^{-1}$. Results of this linear superposition approximation appear as dashed curves in Fig. 2. While adequate for spheres more than 50 radii from the wall [(c) and (d)], linear superposition underestimates the wall's influence for smaller separations [(a) and (b)].

A more complete treatment not only resolves these quantitative discrepancies but also reveals an additional surprising influence of the bounding surface on the spheres' dynamics: the highly symmetric and experimentally accessible modes parallel to the wall are no longer independent.

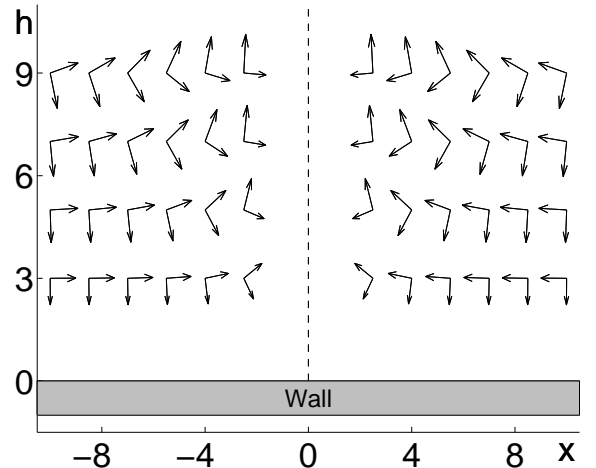


FIG. 3. Cross-sectional view of the diffusive modes for two spheres near a wall. Collective motion normal to the wall becomes increasingly coupled with relative motion parallel to the wall as h approaches r . Collective normal modes at large r cross over continuously to relative parallel modes as r decreases. The dashed line at $x = 0$ indicates the symmetry plane.

The combination of a neighboring sphere and two image systems contribute $b_{i\alpha,j\beta}^e = G_{\alpha\beta}^S(\vec{r}_i - \vec{r}_j) + G_{\alpha\beta}^W(\vec{r}_i - \vec{R}_i) + G_{\alpha\beta}^W(\vec{r}_i - \vec{R}_j)$ to the mobility of sphere i in the α direction. Eigenvectors of the corresponding diffusivity tensor appear in Fig. 3. The independent modes of motion are rotated with respect to the bounding wall by an amount which depends strongly on both r and h . The experimentally measured in-plane motions clearly are not independent yet will satisfy Stokes-Einstein relations, nonetheless, with pair-diffusion coefficients $D_{\alpha}^{C,R}(r, h) = D_{1\alpha,1\alpha}(r, h) \pm D_{1\alpha,2\alpha}(r, h)$, where the positive sign corresponds to collective motion, the negative to relative motion, and α indicates directions either perpendicular or parallel to the line connecting the spheres' centers. Explicitly, we obtain

$$\frac{D_{\perp}^{C,R}(r, h)}{D_0} = 1 - \frac{9}{16} \frac{a}{h} \pm \frac{3}{4} \frac{a}{r} \left[1 - \frac{1 + \frac{3}{2}\xi}{(1 + \xi)^{3/2}} \right] \quad (12)$$

$$\frac{D_{\parallel}^{C,R}(r, h)}{D_0} = 1 - \frac{9}{16} \frac{a}{h} \pm \frac{3}{2} \frac{a}{r} \left[1 - \frac{1 + \xi + \frac{3}{2}\xi^2}{(1 + \xi)^{5/2}} \right] \quad (13)$$

up to $\mathcal{O}(a^3/r^3)$ and $\mathcal{O}(a^3/h^3)$, where $\xi = 4h^2/r^2$. These results appear as solid curves in Fig. 2.

To gauge the success of this procedure and to quantify the range over which the presence of a wall measurably influences colloidal dynamics, we computed the error-weighted mean-squared deviation of the predicted diffusivities from the measured values, $\chi_{\psi}^2(h) = \int \left[\left(D_{\psi}^{expt}(r, h) - D_{\psi}(r, h) \right) / \delta D_{\psi}^{expt}(r, h) \right]^2 dr$. Typical results appear in Fig. 4. The lowest-order stokeslet presented here analysis agrees well with measurement over the entire experimentally accessible range. Deviations from the linear superposition approximation's predictions, on the other hand, are evident out to $h = 15 \mu\text{m}$ or 30 radii.

The present study demonstrates that a confining surface can influence colloidal dynamics over a large range of separations. This influence is inherently a many-body effect, as demonstrated by the linear superposition approximation's failure. Quantitative agreement between our measurements and a leading-order stokeslet analysis offers hope for future progress in understanding confinement's effects on colloidal dynamics.

David Altman developed the transparent thin film heater with support from the MRSEC REU program at the University of Chicago. Work at the University of Chicago was supported by the National Science Foundation through grant DMR-9730189, through the MRSEC program of the NSF through grant DMR-9888595, and by the David and Lucile Packard Foundation. Theoretical work was supported by the A.P. Sloan Foundation, the Mathematical Science Division of the National Science Foundation, and a NDSEG Fellowship to TS.

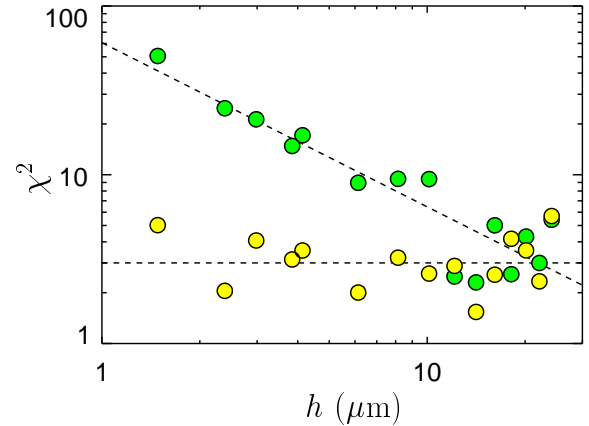


FIG. 4. Mean-squared deviations between measured and predicted diffusion coefficients for relative perpendicular motion, averaged over initial separations r . Leading-order stokeslet analysis yields uniformly good predictions for all accessible values of h . Linear superposition, on the other hand, underestimates the wall's influence. Dashed lines are guides to the eye and emphasize the a/h leading-order correction to the linear superposition model's prediction.

- [1] T. G. M. van de Ven, *Colloidal Hydrodynamics* (Academic Press, San Diego, 1989).
- [2] R. E. Caflisch and J. H. C. Luke, *Phys. Fluids* **28**, 759 (1985).
- [3] J.-Z. Xue *et al.*, *Phys. Rev. Lett.* **69**, 1715 (1992).
- [4] H. Nicolai and E. Guazzelli, *Phys. Fluids* **7**, 3 (1995).
- [5] P. N. Segrè, E. Herbolzheimer, and P. M. Chaikin, *Phys. Rev. Lett.* **79**, 2574 (1997).
- [6] M. P. Brenner, *Phys. Fluids* **11**, 754 (1999).
- [7] J. Crocker, *J. Chem. Phys.* **106**, 2837 (1997).
- [8] J.-C. Meiners and S. R. Quake, *Phys. Rev. Lett.* **82**, 2211 (1999).
- [9] L. P. Faucheux and A. J. Libchaber, *Phys. Rev. E* **49**, 5158 (1994).
- [10] J. Happel and H. Brenner, *Low Reynolds Number Hydrodynamics* (Kluwer, Dordrecht, 1991).
- [11] N. Liron and S. Mochon, *J. Eng. Math.* **10**, 287 (1976).
- [12] L. Lobry and N. Ostrowsky, *Phys. Rev. B* **53**, 12050 (1996).
- [13] D. G. Grier, *Curr. Opin. Colloid Interface Sci.* **2**, 264 (1997).
- [14] J. C. Crocker and D. G. Grier, *J. Colloid Interface Sci.* **179**, 298 (1996).
- [15] M. L. Hair, in *Clean Surfaces*, edited by G. Goldfinger (Marcel Dekker, New York, 1970), pp. 269–284.
- [16] D. S. Viswanath and G. Natarajan, *Data Book on the Viscosity of Liquids* (Hemisphere, New York, 1989).
- [17] K. Sasaki *et al.*, *Opt. Lett.* **16**, 1463 (1991).
- [18] G. K. Batchelor, *J. Fluid Mech.* **74**, 1 (1976).
- [19] D. L. Ermak and J. A. McCammon, *J. Chem. Phys.* **69**, 1352 (1978).
- [20] C. Pozrikidis, *Boundary Integral and Singularity Methods for Linearized Viscous Flow* (Cambridge University Press, Cambridge, 1992).
- [21] J. R. Blake, *Proc. Camb. Phil. Soc.* **70**, 304 (1971).